

Optical Seeing Measurements with an Optical Telescope on a Radio Antenna

Nobuharu UKITA, Bungo IKENOUE, and Masao SAITO
(Received 2007 October 31, Accepted 2008 January 30)

Abstract

Individual images of a video CCD camera with a 10-cm objective lens recorded for pointing performance tests of a prototype 12-m antenna for the ALMA project have been analyzed to evaluate both antenna tracking accuracy and optical seeing at the NRAO VLA site. Data of star image centroid motion have been compared with readouts of angle encoders and inclinometers on the azimuth axis in the yoke structure of the antenna. Under good tracking conditions, a power spectral density (PSD) of image motion during tracking over about 5 minutes had a Kolmogorov power index of $-2/3$. At frequencies > 4 Hz, the PSD showed a steeper decline due to a finite exposure time of the video camera (1/30 seconds) than $-2/3$, which suggests a wind speed of about 3 m s^{-1} at the level where the main turbulence occurs. At lower frequencies, a flattening of the PSD was observed with a turnover frequency of about 0.05 Hz, which in turn suggests an “outer scale” of about 60 m, a length of large-scale disturbances in Kolmogorov’s model. The image centroid fluctuations observed during all-sky pointing tests showed a dependence on air mass A as $A^{0.5}$ and were 0.5 to 0.9 arcseconds rms at the zenith. These measurements suggest that observations for 2–3 seconds can determine a star position with a typical error of 0.3 to 0.6 arcseconds.

Keywords: optical seeing: radio telescope: pointing

1. Introduction

For ground-based astronomy, atmospheric seeing is of great concern, and numerous works both experimental and theoretical have been extensively made (e.g., Hardy, 1998; Roddier, 1999; Avila, 2002). Traditionally single aperture telescopes had been used to estimate seeing quality from star trails recorded on photographs. But they had suffered from wind shakes and telescope tracking errors. In order to avoid these problems, a new technique was developed to measure the relative motion of the two images formed through two small pupils on a common telescope. This technique, differential image motion monitor (DIMM), is inherently insensitive to such errors. Recently DIMMs have been widely used for evaluation of optical seeing for observatory site testings (e.g., Sarazin and Roddier, 1990).

One of key parameters of optical turbulence is the outer scale of refraction index fluctuation obeying Kolmogorov’s “two-thirds law” (e.g., Avila, 2002). The flattening of its spectrum below the outer scale is necessary to represent a finite energy input. While differential methods such as DIMM are only sensitive to high frequency components, interferometric and absolute image motion measurements are sensitive to outer-scale effects (e.g., Martin, 1987; Tokovinin, 2002).

Optical pointing telescopes (OPTs) have become standard equipment on radio antennae for pointing and tracking

diagnosis (e.g., Mangum, 2000; Ezawa et al., 2004; Ukita et al., 2004, hereafter Paper I; Mangum et al., 2006). Recent submillimeter telescopes have achieved high angular resolutions better than 10 arcseconds at their shortest operational wavelengths; and hence they are required to have high pointing accuracy better than one arcsecond. However, atmospheric turbulence causes temporal movements of star image positions, an order of one arcsecond, which seems to make it difficult to measure the antenna pointing/tracking errors with a 0.1 arcsecond accuracy. What they have done and plan to do looks like the classical methods astronomers/engineers had tried a half century back. But time has passed; the understanding of the atmospheric seeing have made much progress and the advent of modern antenna drive technology makes it feasible for an antenna mount to track a star and to scan the sky with a sub-arcsecond accuracy. Therefore an assessment of characteristics of optical seeing over a test site is crucial for planning and execution of antenna pointing performance evaluation. We have revisited the data of stellar images obtained for pointing evaluation tests (Paper I) of a prototype 12-m antenna for the Atacama Compact Array (ACA) of the Atacama Large Millimeter/submillimeter Array (ALMA) project to address characteristics of optical seeing over the NRAO VLA site (34.1° N , 107.6° E) in New Mexico, the United States.

In Paper I, we have described the prototype 12-m ACA antenna and its preliminary test results. Ikenoue et al. (2005,

hereafter Paper II) have reported on our OPT system and a detailed evaluation results. In this paper, we focus on characteristics of centroid motion of star images. Section 2 briefly describes our antenna pointing system and OPT system. We show our analyses of both optical seeing at the VLA site and tracking errors of the prototype antenna. Section 3 discusses power spectral density (PSD) of star image motion. Detailed analyses have revealed a flattening of the PSD with a turnover frequency of about 0.05 Hz, which seems to be related to the outer scale effect. Section 3 also discusses achievable measurement accuracies under actual seeing conditions. And we demonstrate that the OPT system on the radio antenna is a powerful diagnosis tool to reveal tracking errors such as stick-slip friction error, tiltmeter output oscillation, and abnormal oscillation of the antenna control servo-loop.

2. Equipments and Measurements

2.1 An Optical Pointing Telescope and an Antenna under Test

The optical pointing telescope was a 10-cm diameter refractor with a focal length of 920 mm and a 2X extender lens that gives a final focal length of 1840 mm on a peltier cooled CCD camera (Cohu 4920). The telescope tube and a support tripod to the central hub of the antenna main reflector structure were made of invar to minimize flexure due to thermal deformation. The telescope was of the NRAO

design (Mangum, 2000; and Mangum et al., 2006), however the image acquisition system (Paper II) was our own style. Since eigenfrequencies of the antenna in azimuth and elevation are about 6 Hz, it is useful to record each video frame image at 30 Hz to detect tracking errors associated with these frequencies, if any. The video signal was digitized with a frame grabber of 8 bit (National Instruments, Model NI1407), and recorded on a PC (DELL Optiplex GX260) in a bitmap image format of 640×480 pixels. The data rate of 0.5 Gbyte per minute is high, which is, however, a piece of cake for a storage device of modern computers. The plate scales were 1.16 arcsecond per image pixel in both horizontal and vertical. A typical star image size (FWHM) was about 2 to 4 arcseconds. A red filter (R64) was used to make observations during daytime. An effective wavelength was estimated to be 740 nm from response curves of the CCD and the filter.

The OPT was installed on the ACA 12-m antenna which was built at the NRAO VLA site at an elevation of 2120 m. The antenna site is located near the center of the Plains of San Agustin in New Mexico, a flat highland of a vast extent of about 30 km. The antenna has an alt-azimuth mount (figure 1). The ALMA specification of "absolute" pointing accuracy for the whole sky is 2.0 arcseconds rss. It also requires offset pointing accuracy of 0.6 arcseconds rss for 4 degrees for 15 minutes. The maximum speeds are 6 and 3 degrees s^{-1} in azimuth and elevation, respectively. The maximum accelerations are 24 and 12 degrees s^{-2} in azimuth and elevation. The antenna has angle encoders of a 360 deg/25 bit resolu-

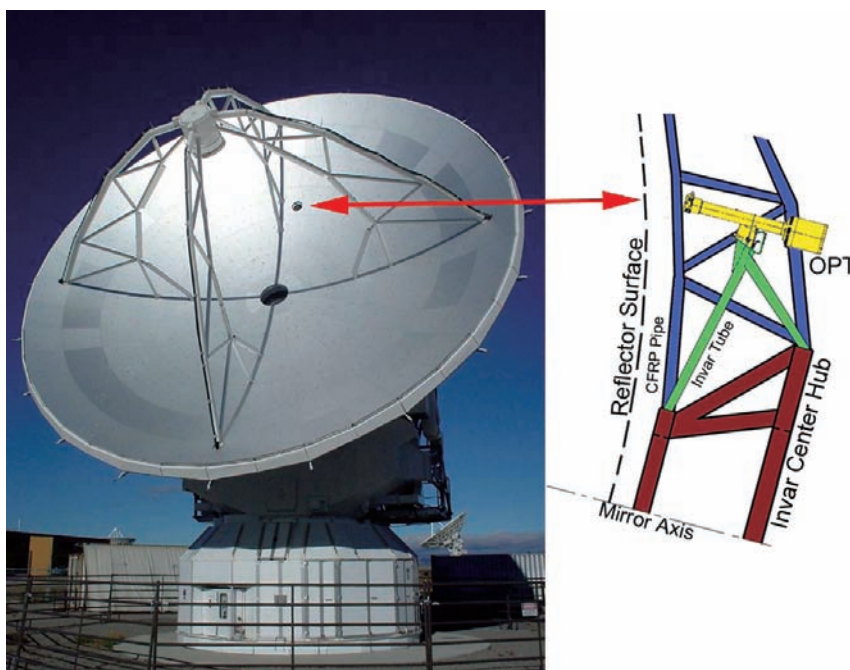


Figure 1: The ACA prototype 12-m antenna under test. A 10-cm optical pointing telescope (OPT) is located behind a hole indicated. The OPT tube and a support tripod as well as the reflector back-up structure are made of low thermal-expansion material.

tion and 40 milli-arcseconds (mas) calibration accuracy (Ukita et al., 2001). Two servo-inclinometers (Shinko Denki, Model LSO-C1) were used to detect tilt variation of the azimuth axis due to thermal deformation of the pedestal mount structure and runout motion of an azimuth bearing, namely erroneous motion related to imperfect raceway grooves of a bearing. It incorporates a pendulum and an actuator coil with a servo circuit of force-balance closed-loop configuration. Inclination is proportional to the amount of feed-back. It has a response frequency of about 1 Hz. It is located on the azimuth axis in the yoke structure to avoid the centrifugal force of the antenna azimuth rotation.

The OPT is rigidly fastened to the central hub of the main reflector (figure 1). Vibration measurements with accelerometers on both the OPT and the backup structure of reflector have shown that they oscillate with the same amplitude and phase in frequencies $<$ about 18 Hz (see figures 4 and 5 of Paper II). Major components of the vibration were around 5 and 6 Hz, related to the natural frequencies of the antenna structure. Typical amplitudes were about 50 mas rms, which is not detrimental. The OPT had oscillations of its own near 31 and 45 Hz with an amplitude of 23 mas rms. Since these higher frequency components are smoothed out by a finite frame exposure time of 1/30 seconds, the error due to the OPT vibration is significantly reduced to $<$ 2 mas.

2.2 Continuous Tracking Measurements

Five runs of tracking of α Gem were made in the nights

of December 6 and 7, 2003. CCD images were continuously recorded for about five minutes. The 30 frames per second (fps) has actually been reduced to 24 fps due to missing frames. Command positions and encoder readouts were also recorded every 48 milli-second. During the runs, the star were at elevation angles of 65 to 75 degrees. The wind speeds at 9 m from the ground were about 1 m s^{-1} . Figure 2 is a sample of the data recorded from 8h21m to 8h26m of December 7 (UT). The upper panel shows a time history of the star positions in elevation; and the lower panel displays elevation servo error which is differences between encoder readout and sum of command position and pointing model correction. The standard deviations of the star positions were 0.6 arcseconds in both azimuth and elevation. Those of the servo errors range from 10 to 20 mas in azimuth and from 30 to 70 mas in elevation.

Averaged PSDs of the image centroid motion and the servo error in the azimuth and elevation directions for the five runs are shown in figures 3a and 3b, respectively. The PSD of image motion basically showed a Kolmogorov power index of $-2/3$. At frequencies $>$ 4 Hz, the PSD showed a steep decline which had a power index of $-1.54 \pm 0.07 (3\sigma)$. At lower frequencies, a flattening of the PSD was discernible, except for the lowest two data points (open circles in figure 3a). A vertical red arrow indicates a typical measurement error estimated from standard deviations of the 10 measurements for individual frequency channels divided by square root of the number of measurements. To estimate an effect of a secular tracking drift error, we show a PSD of a

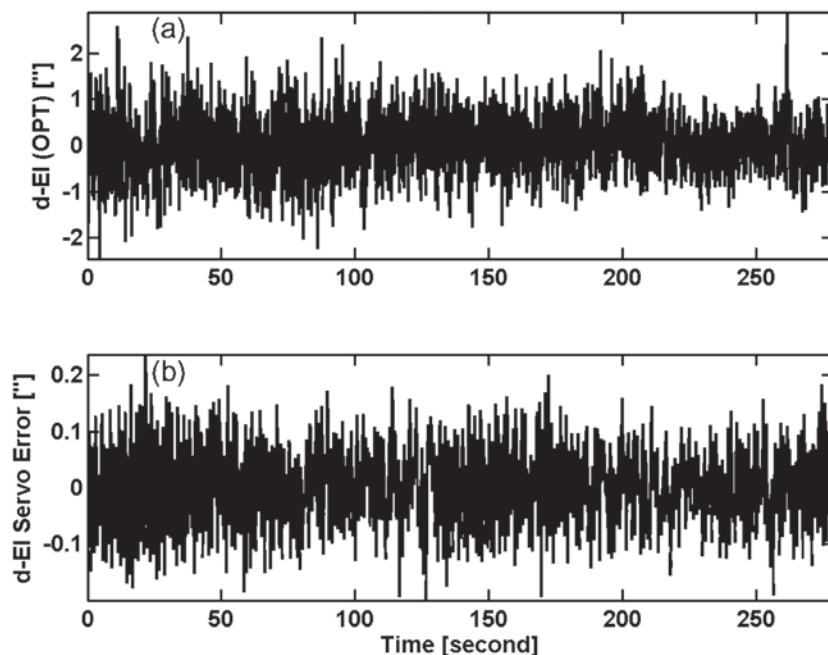


Figure 2: Time histories of optical image motion and antenna servo error.

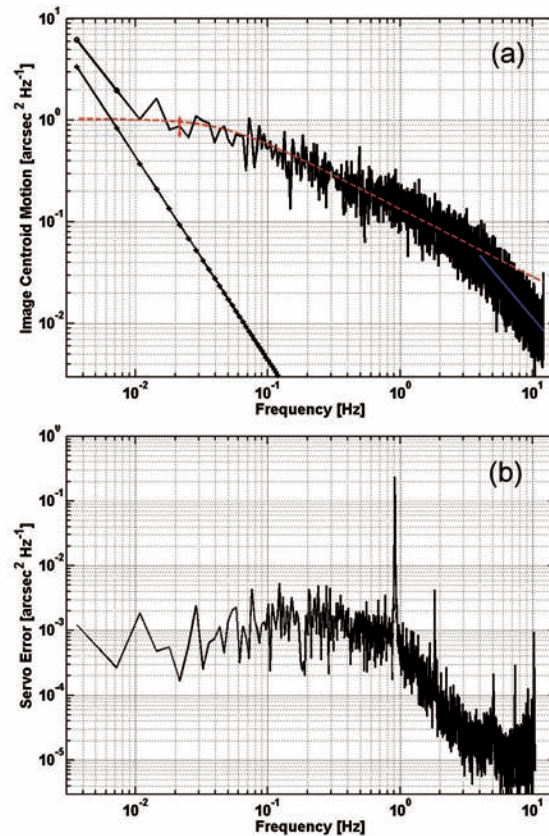


Figure 3: (a) an average spectrum of 10 PSDs of the optical image motion in azimuth and elevation directions. A vertical red arrow indicates a typical measurement error at lower frequency region. A model spectrum (dashed red line) that accommodates a von Karman spectrum is fit to the observed PSD. The blue line indicates a fit to the PSD at frequencies > 4 Hz. A straight line with + marks is a PSD of a secular tracking drift error of 0.35 arcseconds per 5 minutes. (b) an average PSD of the servo error. A sharp component in the servo error at 0.9 Hz was seen only in the error in elevation.

secular drift of 0.35 arcseconds per 5 minutes (a straight line with + marks). The PSD in the lower frequencies < 2 Hz is fitted to a following empirical equation:

$$F(\nu) = A(\nu^2 + \nu_0^2)^{-1/3},$$

where A is a constant and ν_0 is a turnover frequency. We have found that the turnover frequency to be 0.047 ± 0.012 (σ) Hz. The estimate of uncertainty has been made by using 100 PSD data sets which are generated by randomly adding the measurement errors mentioned above.

The PSD of the servo error was much smaller than that of the image motion except for a sharp component at 0.9 Hz. It was seen only in the error in elevation. We have tried to identify the source of this error, but we have failed.

2.3 All-Sky Pointing Measurements

All-sky pointing measurements were made over nine nights in 2004 March and one daytime in 2004 June. A total of 14 runs of the measurements (Table 1) were obtained along with logging data of command positions and readouts of the angle encoders and the servo-inclinometers. Each run

consisted of 1 to 3 sub-runs of 20 to 25 minutes in which about 70 stars were measured. Each star, brighter than $m_v < 3.5$ magnitudes, was observed for 1.8 to 3.6 seconds.

Figure 4 shows an example of measurement data towards Polaris on March 20, 2004. Figures 4a and 4b display star trails for 2.7 seconds in azimuth and elevation, respectively. Figures 4c and 4d are differences between angle encoder readouts and commanded angles corrected for pointing model. This quantity includes both servo errors and offset values which the control circuit calculates based on data of the metrology system such as inclinometers. This quantity is a little bit confusing. But we did not have proper tapping points to monitor offset values in the control circuit. Figures 4g and 4h are outputs of inclinometer readout in cross-elevation axis and in elevation axis, respectively. Under a normal operation condition, the inclinometer output is expected to have a nearly constant value for a short period. The figure 4g seems to display such a condition. Therefore we blame the servo-loop for a "stop-and-go" behavior seen in figure 4c. The sawtooth shape is typical for servo error due to non-linear friction torque variation at low speed, referred to as "stick-slip", in the azimuth bearing.

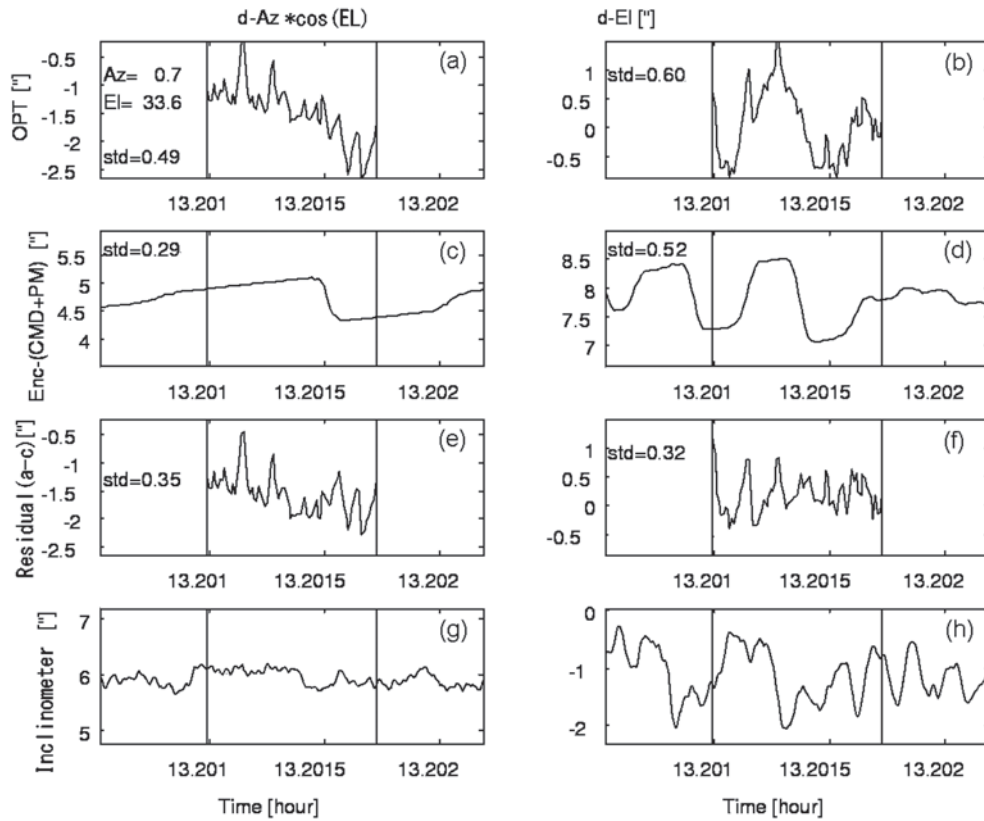


Figure 4: A sample of all-sky pointing measurement data for Polaris on March 20, 2004. (a) Image centroid trail measured with the OPT, (c) servo error, (e) star position fluctuation after subtraction of the servo error in azimuth. (g) Inclinometer readout of cross elevation axis. (b), (d), (e), and (h) in elevation.

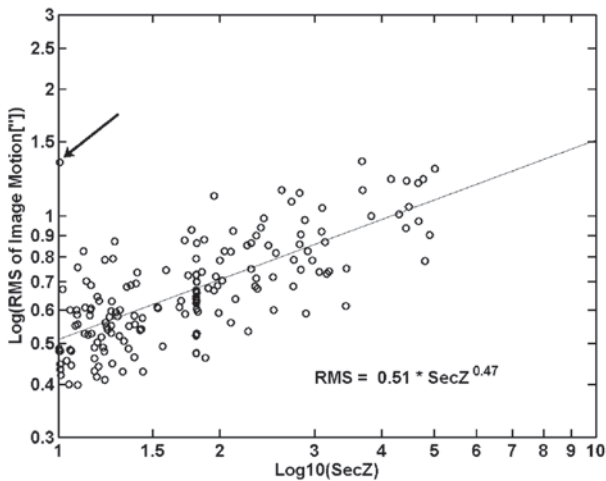


Figure 5: Zenith angle dependence of standard deviations of image motion. An arrow indicates a measurement which has shown abnormal oscillation (see Appendix-B)

On the other hand, the inclinometer output in elevation displayed a large unsteady variation (figure 4h). There is a close resemblance between a rectangular pattern of the offset time history (panel d) and an low-pass filter output time profile expected from the inclination readouts. Also there is a close resemblance between the rectangular pattern (figure 4d) and the observed star trail pattern (figure 4b). These

strongly suggest that the antenna mount itself was stable but the inclinometer for elevation produced a factitious output oscillation excited by a large deceleration just before the antenna reaches to a target star. As a result, the antenna deviated from the target star. Since the inclinometers sit on the azimuth axis, they may not receive unwanted acceleration in azimuth rotation. But the fast motion in elevation pushes the yoke base, and the inclinometer for elevation may receive unwanted acceleration. The considerations suggest that differences between the time profiles of figure 4a and 4c and between those of figure 4b and 4d, shown in figure 4e and 4f, seem to be true components of image motion due to atmospheric seeing.

Figure 5 shows standard deviations of the image motion described in the previous paragraph against air mass. Figures for all 14 runs are shown in Appendix-A. A thin line indicates a least square fit of them. At the zenith, the standard deviations of image position was 0.51 arcseconds. A power index was 0.47, which is close to the expected value of 0.5.

Table 1 lists these values thus obtained for the 14 measurement runs. The fifth column gives the variances at the zenith, the sixth column the power indices, the seventh column root mean square of individual variances for each run,

Table 1. Stellar Image Motion at the VLA site

Date	UT (LT = UT-7h)	Optical Seeing						Servo Error			
		SecZ a*SecZ ² b	RMS of individual STDs	Wind Velocity	Number of frames	Accuracy of Error Estimate	(Az)	(El)	(radial)		
2004 mdd	hh:mm - hh:mm	(#)	a ["]	b ["]	(radial) ["]	[m/s]		(radial) ["]	["]	["]	["]
314	07:00 - 07:49	a	0.50	0.64	0.86	1 - 3	50	0.39	0.13	0.30	0.32
314	10:36 - 12:25	b	0.56	0.56	0.90	1 - 4	50	0.41	0.13	0.25	0.28
315	08:20 - 09:15	c	0.86	0.51	1.30	3 - 8	50	0.59	0.14	0.24	0.28
316	06:16 - 07:11	d	0.83	0.55	1.30	1	100	0.53	0.15	0.28	0.31
316	11:01 - 12:04	e	0.70	0.53	1.07	3 - 4	100	0.43	0.14	0.25	0.29
316	12:22 - 13:17	f	0.68	0.57	1.06	3 - 6	100	0.42	0.16	0.26	0.31
317	05:09 - 05:53	g	0.63	0.68	1.15	3 - 5	100	0.46	0.15	0.30	0.33
318	06:06 - 07:13	h	0.57	0.68	0.97	3 - 5	75	0.41	0.15	0.31	0.34
319	06:34 - 07:17	i	0.72	0.64	1.24	3 - 4	75	0.52	0.15	0.29	0.33
319	08:44 - 09:49	j	0.54	0.52	0.82	2	75	0.35	0.15	0.29	0.33
319	12:38 - 13:34	k	0.46	0.59	0.70	1	75	0.30	0.18	0.27	0.32
320	12:38 - 13:30	l	0.51	0.47	0.73	0 - 1	75	0.31	0.16	0.28	0.32
320	16:16 - 16:55	m	0.65	0.73	1.15	0 - 1	75	0.49	0.16	0.29	0.33
616	04:59 - 06:21	n	0.73	0.41	1.05	3 - 5	50	0.48	0.17	0.24	0.29

#) Notation in figures A-1, A-2, and A-3 in Appendix-A

the eighth column wind velocities during the measurements. The 11th and 12th columns list the variances of servo errors in azimuth and elevation, respectively, during the OPT measurement periods as indicated by vertical lines in the figures 4c and 4d. They are typically 150 mas in azimuth and 300 mas in elevation. These errors just after arrival to a target position are a factor 10 larger than those during steady tracking shown in figure 2b (10 – 70 mas).

An arrow in figure 5 indicates one star of unusually a large variance which has prompted us to look for additional sources of error. It was a 5 Hz vibration of the telescope mount in the azimuth. This is another example of antenna tracking diagnosis by the OPT. For an interested reader(s), we show the event in Appendix-B.

3. Discussion

Use of a single aperture telescope for seeing study has long been considered not to be practical, because it is sensitive to pointing error (e.g., Tokovinin, 2002). In figure 3a, we show a sample PSD of a secular tracking drift error of 0.35 arcseconds per 5 minutes, namely 1 arcsecond per 15 minutes. If an antenna had solely this tracking error, it barely meets the ALMA specification for "offset" pointing performance to be better than 0.6 arcseconds rms. In fact, it is a tough task for an antenna in the open air to achieve such high pointing performance imposed by ALMA. Our PSD of image motion at the lowest frequencies (indicated by open circles) in figure 3a apparently suggests that our antenna was affected by such a level of tracking drift and that we need to improve its tracking accuracy. A source(s) of the error is presumably thermal deformation of the mount structure and/

or an imperfect pointing model we used.

The PSD shown in figure 3a displays the deviations at the both ends of frequency range from a Kolmogorov power dependence of $-2/3$. Martin (1987) have discussed an effect of finite exposure time on PSDs of image motion. He has shown theoretical PSDs under various wind speeds measured with a 10-cm telescope and 1/30 seconds exposure. We have compared our PSD with them, and have estimated the wind speed at the level where the main turbulence occurs to be about 3 m s^{-1} . On the other hand, the flattening of the PSD at lower frequencies indicates the turnover frequency to be 0.05 Hz. From the inferred wind speed and turnover frequency, we derive a scale length of about 60 m, which corresponds to an "outer scale" of turbulence related to the largest size perturbations in von Karman turbulence model. The outer scale estimated from our single aperture telescope is in the range of reported ones from 10 to 100 meters measured by other methods (e.g., Ziad et al., 2000).

The observed PSD of image motion suggests an OPT is a powerful tool for antenna tracking diagnosis. For example, Ukita et al. (2006a and 2006b) have found a wind shake of the antenna mount with an amplitude of about a few arcseconds and frequency of 0.15 Hz. The PSD yaw motion of the elevation axis due to wind loading was about $7 \text{ arcsec}^2 \text{ Hz}^{-1}$ at 0.15 Hz. This wind shake is larger than that of the stellar image motion, and can be detected with the OPT. And how to minimize such wind loading effects with a metrology system is a core technology of modern submillimeter antennae requested by ALMA.

For "absolute" and "offset" pointing performance evaluations, we need to give an estimate of position measurement accuracies achieved by a typical 2 – 4 seconds observations

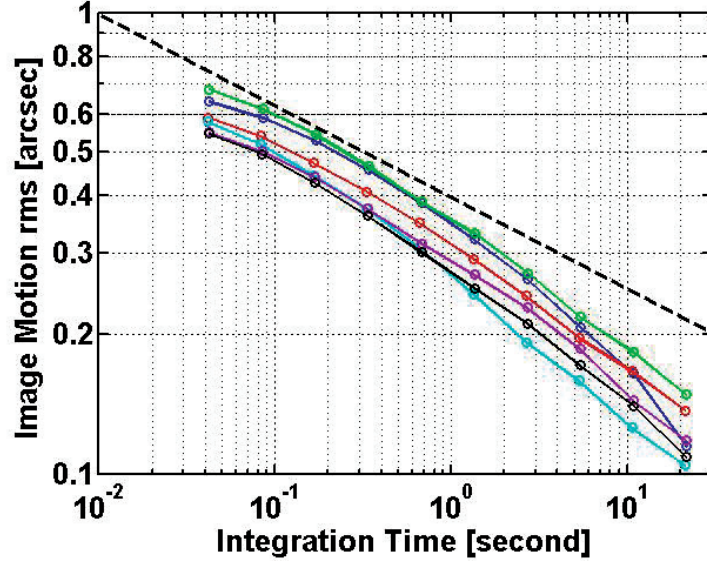


Figure 6: Improvement of position determination accuracy with a number of images for averaging. A dashed line indicates a slope of -0.2 expected for time series data with a Kolmogorov spectrum.

under actual seeing conditions. As shown in the section 2.2, the time series data of the continuous tracking of α Gem are dominated by seeing fluctuation. After averaging $N (= 2^n; n=0, 1, 2, \dots)$ bins of the time series data for about five minutes, we calculate their standard deviations. Figure 6 shows them against number of images (total time of exposure). A dashed line in the figure indicates a slope of -0.2 expected for time series data with a Kolmogorov PSD. A decline for the first few dots is slower than the slope of -0.2 due to the smaller power in the PSD spectrum at high frequency. A decline for the longer exposure time (1 seconds) becomes faster than -0.2 due to the flattened PSD spectrum at low frequency. These suggest that position measurement errors basically follows the slope of -0.2 . We can predict an error of positional determination from the number of $1/30$ second frames of consecutive exposures and its standard deviations. The 9th column of table 1 lists the numbers of CCD image frames recorded. The average accuracies of star position measurement of all the measurements for each run are listed in the 10th column. They were 0.3 to 0.6 arcseconds.

In summary, from the PSD of star image motion observed with a 10-cm single aperture telescope, we have derived that the "outer scale" of turbulence over the VLA site was about 60 m. The optical seeing at the VLA site is generally good enough to evaluate the pointing performance of the antenna designed for submillimeter observations.

Antenna Test Facility in the VLA site. They are very grateful to the referee for a careful reading of the manuscript and insightful and penetrating suggestions.

The authors thank NRAO staff and members of Antenna Evaluation Group of ALMA for their kind support at the

A Zenith angle dependence of stellar image motion

Figures A-1 and A-2 show a zenith angle dependence of variances of star image motion observed the OPT for 2 – 4

seconds to estimate a variance at the zenith. A thin line indicates a least square fit of them. Notations in each panel correspond to those shown in Table 1.

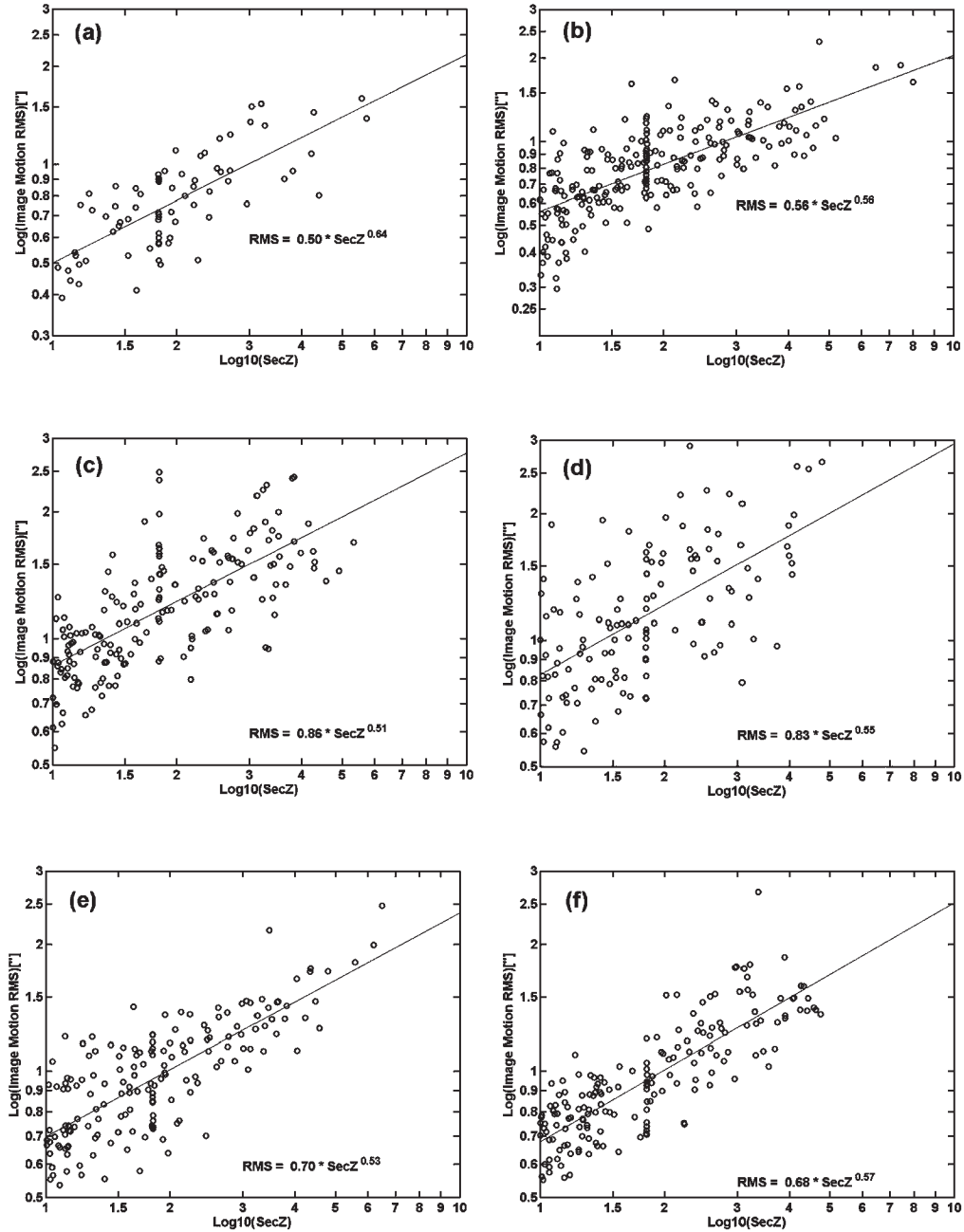


Figure 7: Zenith angle dependence of variances of star image motion observed for a few seconds.

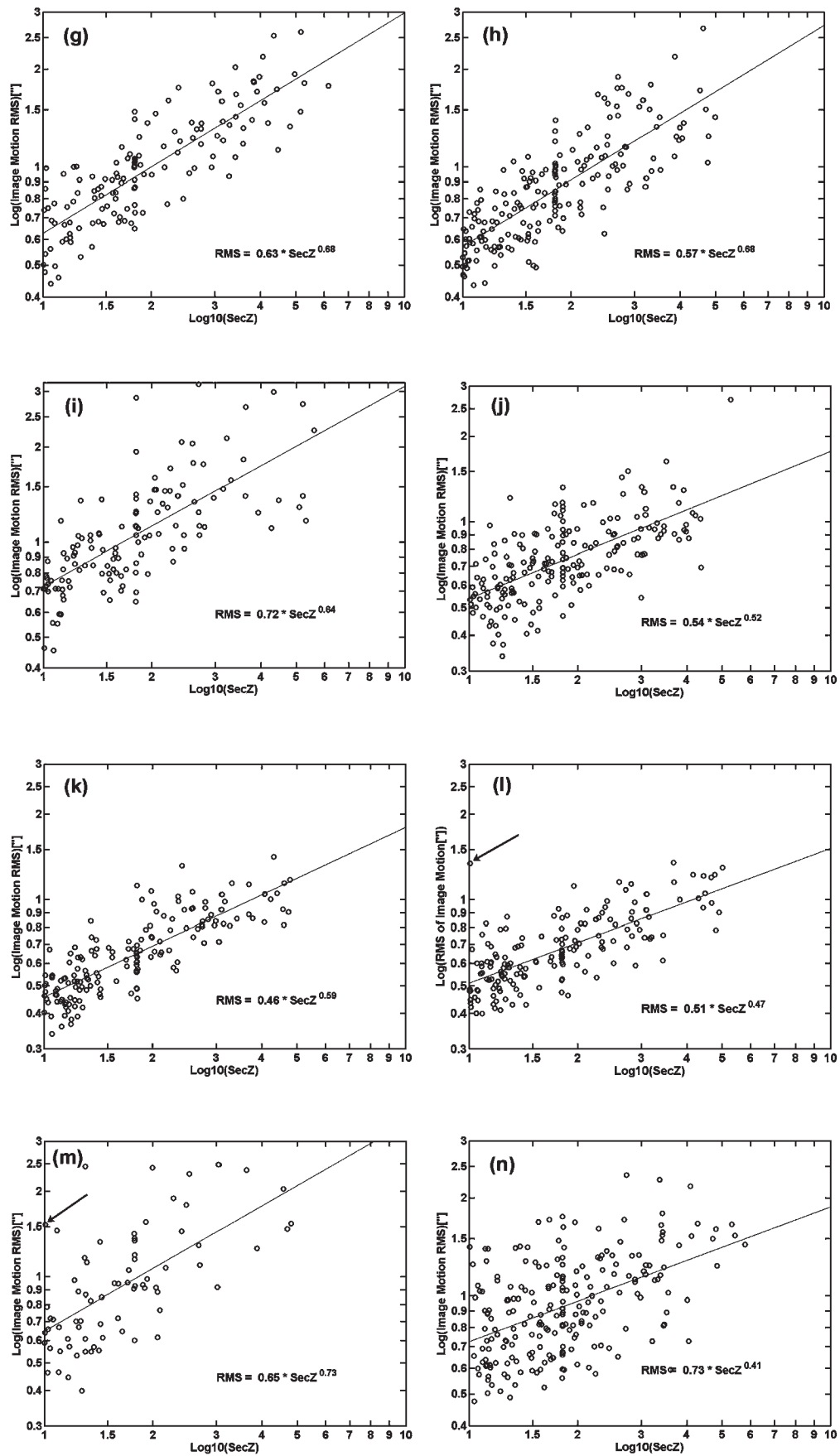


Figure 8: Same as figure A-1, but for measurement runs with notations (g) to (n) in Table 1. Arrows in panel (l) and (m) indicate measurements which have shown abnormal oscillations (see Appendix-B).

B Abnormal Oscillation

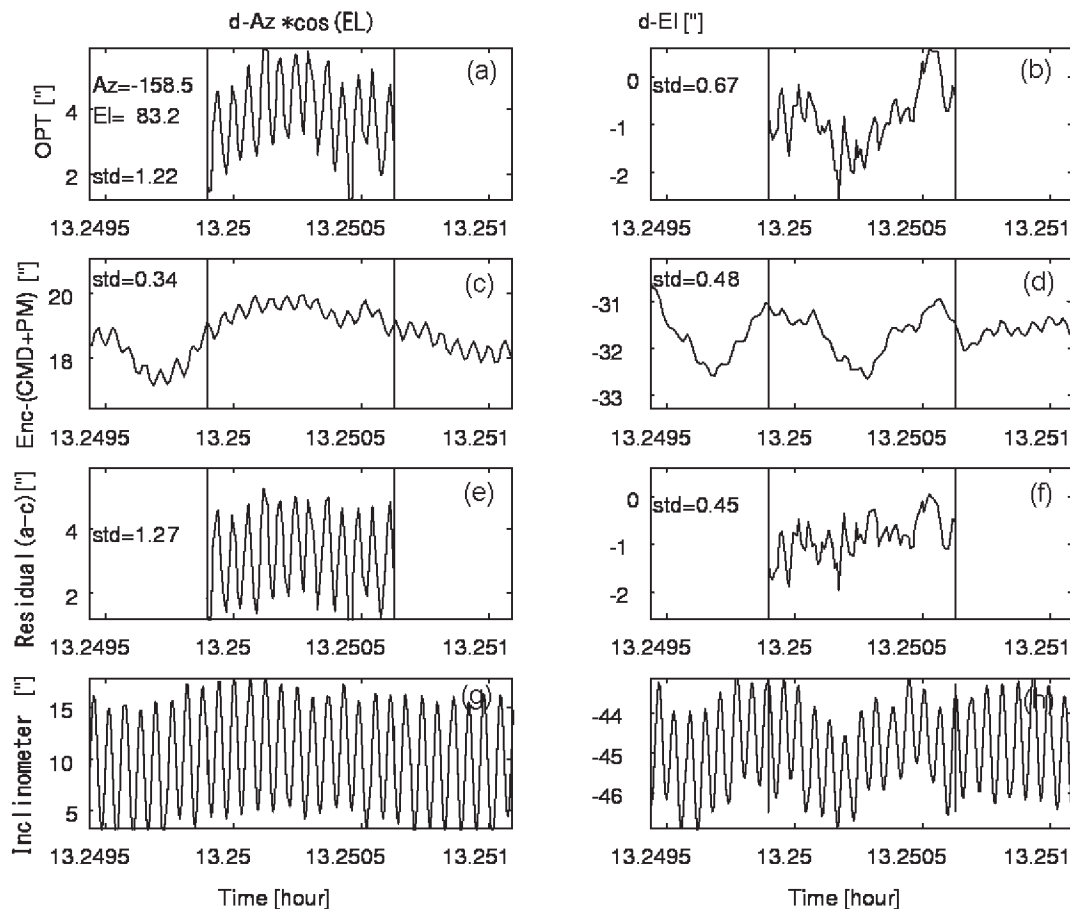


Figure 9: An example of an unusually large oscillation of the antenna mount structure detected by the OPT.

References

- Avila, R. 2002, "Observational methods for the study of optical turbulence", *ASP Conference Proc.*, **266**, 48-63.
- Ezawa, H., Kawabe, R., Kohno, K., and Yamamoto, S. 2004, "The Atacama Submillimeter Telescope Experiment (ASTE)", *Proc. SPIE*, **5489**, 763-772.
- Hardy, J.W., 1998, "Adaptive Optics for Astronomical Telescopes", *Oxford Series in Optical and Imaging Sciences*, Oxford University Press, USA.
- Ikenoue, B., Ukita, N., Saito, M., Ezawa, H. 2005, "Performance evaluation of an ALMA 12-m prototype antenna with an optical pointing telescope system", *Report Natl. Astron. Obs. Japan*, **8**, 111-123 (in Japanese).
- Mangum, J.G., 2000, "An Optical Pointing Telescope for the ALMA Prototype Antennas", ALMA Memo, #288, <http://www.alma.nrao.edu/memos/>
- Mangum, J.G., et al. 2006, "Evaluation of ALMA Prototype Antennas", *Publ. Astron. Soc. Pacific*, **118**, 1257-1301.
- Martin, H. M. 1987, "Image Motion as a Measure of Seeing Quality", *PASP*, **99**, 1360-1370.
- Roddier, F. 1999, *Adaptive Optics in Astronomy*, Cambridge University Press.
- Sarazin, M., Roddier, F. 1990, "The ESO differential image motion Monitor", *Astron. Astrophys.*, **227**, 294-300.
- Tokovinin, A. 2002, "From Differential Image Motion to Seeing", *PASP*, **114**, 1156-1166.
- Ukita, N. et al., 2001, "A High-Precision Angle Encoder for a 10-m Submillimeter Antenna", *Publ. Natl. Astron. Obs. Japan*, **6**, 59-64.
- Ukita, N. et al. 2004, "Design and performance of the ALMA-J prototype antenna", *Proc. SPIE*, **5489**, 1085-1093.
- Ukita, N. et al. 2006a, "Periodic Vortex Shedding from a 12-m Antenna", *Proc. of National Symposium on Wind Engineering*, **19**, 389-394.
- Ukita, N. et al. 2006b, "Vortex shedding from a 12-m antenna", *Proc. SPIE*, **6267**, 122-129.
- Ulich, B.L. and Davison, W. 1985, "Seeing Measurements on Mount Graham," *PASP*, **97**, 609-615.
- Ziad, A., Conan, R., Tokovinin, A., Martin, F., Borgnino,

J. 2000, "From the grating scale monitor to the generalized seeing monitor", *Appl. Opt.*, **39**, 5415-5425.